

Probing top-partners in Higgs + jets

Andrea Banfi^a, Adam Martin^{b,c} and Verónica Sanz^a

^a*Department of Physics and Astronomy, University of Sussex, Brighton BN1 9QH, UK*

^b*Department of Physics, University of Notre Dame, Notre Dame, IN 46556, USA*

^c*Theory Division, Physics Department, CERN, CH-1211 Geneva 23, Switzerland*

E-mail: a.banfi@sussex.ac.uk, adam.martin@cern.ch, v.sanz@sussex.ac.uk

ABSTRACT: Fermionic top-partners arise in models such as Composite Higgs and Little Higgs. They modify Higgs properties, in particular how the Higgs couples to top quarks. Alas, there is a low-energy cancellation acting in the coupling of the Higgs boson to gluons and photons. As a result of this cancellation, no information about the spectrum and couplings of the top-partners can be obtained in $gg \rightarrow h$, just the overall new physics scale f . In this paper we show that this is not the case when hard radiation is taken into account. Indeed, differential distributions in Higgs plus jets are sensitive to the top-partner mass and coupling to the Higgs. We exploit the transverse momentum distribution of the hard jet to obtain limits on the top-partners in the 14 TeV LHC run, finding that 300 fb⁻¹ of data of 14 TeV LHC are sufficient to rule out top-sector mixing angles $\sin^2(\theta_R) > 0.05$ for top-partners with masses from 300 GeV to above 2 TeV.

Contents

1	Introduction	1
2	Top-partners	3
2.1	Mass matrix	3
2.2	Low energy Higgs theorems and the insensitivity of the hgg coupling	4
3	Top-partners in pseudo-Goldstone Higgs models	5
3.1	Current bounds	6
4	The process $pp \rightarrow H + j$	7
4.1	Generalities	7
4.2	Matrix Element level	9
4.3	Including the effect of PDFs and running	9
5	Stability against higher order corrections and experimental uncertainties	14
6	Mass limits on top-partners	15
7	Conclusions	17
A	Choices in Model Space	18

1 Introduction

The idea that the Higgs is a composite resonance, manifestation of the breaking at high energies of a global symmetry is an old one [1]. This idea has been thoroughly explored and explicit realizations are built as Little Higgs (LH) [2], Composite Higgs (CH) [3] and Partial compositeness [4] models. In these models, the pseudo-Goldstone nature of the Higgs explains why other resonances of the new sector have not been seen yet, but introduces the hurdle of how to generate a potential for the Higgs, a mass and self-interactions. Successful electroweak symmetry breaking requires new states to generate a sizable potential, and those are typically top-partners. Top-partners are heavy resonances with the same quantum numbers as the top and couple strongly to the Higgs. Their contribution is essential to raise the Higgs mass to acceptable levels.

Top-partners are then a key piece to understand electroweak symmetry breaking, but searching for them is more complicated than one would expect. Although they contribute to the hgg coupling, there is a cancellation at low energies which renders this coupling insensitive to the mass and coupling of the top-partner [5, 6]. Instead, the coupling is only sensitive to v^2/f^2 , where f is the scale of breaking of the global symmetry leading to

the pseudo-Goldstone sector. As a result, fits on the rates of Higgs production and decay into various final states are only sensitive to this parameter [7, 8], and not to the individual coupling and mass of the top-partners. Double Higgs production $pp \rightarrow hh$ [9] is one obvious place to look for signs of top-partners. However, this process has a small cross section that is largely insensitive to finite top-partner masses.

Top-partners can be searched for directly, both produced in pairs $pp \rightarrow T\bar{T}$ and singly produced $pp \rightarrow T + X$. However, direct production carries more model dependence since the search strategies and limits depend on how the top-partner decays – an aspect of the model usually unrelated to electroweak symmetry breaking. Most experimental searches focus on the decay modes $T \rightarrow W^+b$, $T \rightarrow Zt$, and/or $T \rightarrow ht$. The bounds, assuming these three modes are the only ones available are roughly 700 – 800 GeV [10]. However if there are other decays possible, such as to exotic pseudo-Goldstone states [11, 12], the T width will increase and the bounds will weaken.

Associated top-partner plus Higgs production $pp \rightarrow T\bar{T}h$ is one way to directly test the hTT coupling. However, the cross section for this process falls steeply as the top-partners become heavy. Additionally, this method requires reconstructing the T produced with the Higgs, which is sensitive to the model-dependent details of how T decays.

In this paper we show that, unlike $pp \rightarrow h$, the process $pp \rightarrow$ Higgs plus high- p_T jet is sensitive to the individual coupling and mass of the top-partner. The reason for this can be seen by inspecting the diagrams that contribute to $pp \rightarrow h + j$. One contribution comes from box diagrams, shown on the left in Fig. 1. As the additional gluon probes the fermion loop, it is not surprising that these diagrams carry a dependence on the fermion mass. The second contribution to $pp \rightarrow h + j$ comes from familiar hgg triangle diagrams stitched on to additional partons. Because of their similarity to $gg \rightarrow h$ diagrams, one may think these diagrams are not sensitive to the internal fermion mass. This is not true; to make a final state with high- p_T , the intermediate gluon in diagrams such as the right side of Fig. 1 must have high virtuality. The high virtuality of the incoming gluon means the fermion triangle is resolved at a different, shorter scale compared to $gg \rightarrow h$ production, and the process becomes sensitive to the fermion mass. Therefore, by studying $pp \rightarrow h + j$ and comparing to SM rates, one can bound the top-partner and its Higgs coupling independent of the details of the T decay.

The setup for the remainder of this paper is as follows: In Sec. 2, we describe the low-energy cancellation at the level of dimension-six operators, and how the extra jet would come from an effective theory including dimension-eight operators. We also set the notation and translation between our parametrization and common models in the literature. In Sec. 4, we show that the sensitivity to mass and couplings arise as double logarithmic terms in the matrix element in the high- p_T limit. We then numerically study $h + j$ production, both at parton level and after including parton distribution functions. In Sec. 5 we discuss the stability of our results at leading order when higher order corrections and experimental uncertainties would be included. Finally, in Sec. 6, we use the differential distributions to set limits on the top-partner masses and couplings in the 14 TeV LHC run.

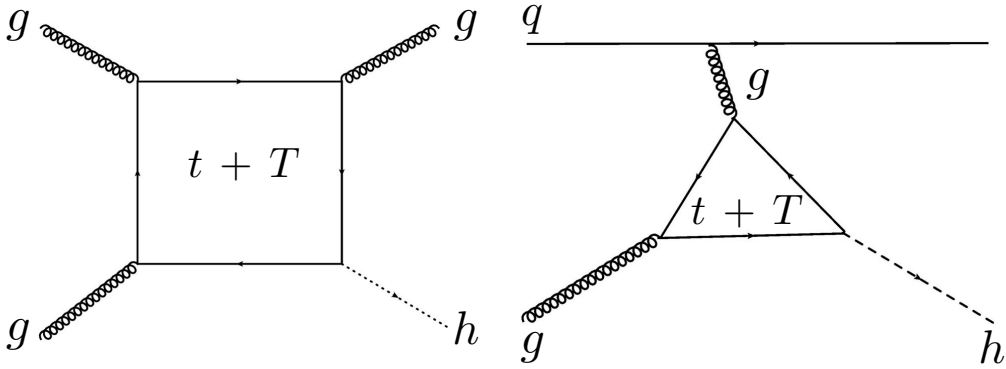


Figure 1. Typical diagrams contributing to $pp \rightarrow h + j$.

2 Top-partners

In this section we describe the effects on Higgs production due to a new colored fermion that mixes with the top quark, which we will call the *top-partner*. To set limits, we present a explicit choice of mass mixing, which can be mapped into from several CH and LH models. Our study will focus on the Higgs production in association with jets, and, in the next section, we explain why one requires extra hard radiation.

2.1 Mass matrix

In this section we parametrize the top-partner sector as a Dirac fermion $T = (T_L, T_R)$, with mass M and a mixing with the SM top given by Δ . Without loss of generality, one can then write the mass matrix between the top $t_{L,R}$ and top-partner $T_{L,R}$ as

$$(\bar{t}_L \bar{T}_L) \begin{pmatrix} \frac{y_{th}}{\sqrt{2}} & \Delta \\ 0 & M \end{pmatrix}_{h=v} \begin{pmatrix} t_R \\ T_R \end{pmatrix}. \quad (2.1)$$

This mass matrix can be diagonalized by a bi-unitary transformation, on the left with a mixing angle of θ_L and on the right with a mixing angle of θ_R . Identifying $\frac{y_{tv}}{\sqrt{2}} = m$, we can trade the three parameters m, Δ, M for the two mass eigenstates m_t, M_T and one of the mixing angles θ_R . Expanding the Higgs about its vacuum expectation value, we can then find the couplings of the mass eigenstate top-quark/top-partner to the Higgs boson. The diagonal Higgs couplings in terms of m_t, M_T, θ_R are:

$$h \bar{t} t : \frac{m_t}{v} \cos^2(\theta_R), \quad h \bar{T} T : \frac{M_T}{v} \sin^2(\theta_R), \quad (2.2)$$

where

$$\theta_R = \frac{1}{2} \arcsin \left(\frac{2m_t M_T \eta}{M_T^2 - m_t^2} \right), \quad \tan \theta_L = \frac{M_T}{m_t} \tan \theta_R \quad (2.3)$$

and $\eta = \Delta/M$.

From the coupling expressions in Eq. (2.2), we can quickly see that the $gg \rightarrow h$ amplitude is insensitive to the mixing angle θ_R . The $gg \rightarrow h$ amplitude from a single fermion loop can be written as [13]:

$$A_i(gg \rightarrow h) = \frac{\alpha_s m_H^2}{4\pi v} \kappa \left(\frac{2 - 4m_{f,i}^2(1-\tau)C_0(4m_{f,i}^2\tau; m_{f,i}^2)}{\tau} \right) \equiv \frac{\alpha_s m_H^2}{4\pi v} \kappa \mathcal{A}_i, \quad (2.4)$$

where $\tau = \frac{m_H^2}{4m_{f,i}^2}$, $\kappa = y_{f,i} \left(\frac{v}{m_{f,i}} \right)$ and C_0 is the three-point Passarino-Veltman function, see Ref. [13] for conventions and the explicit form of C_0 . When the fermion running in the loop is heavy ($\tau \rightarrow 0$), \mathcal{A}_i asymptotes to a constant value, $\mathcal{A}(0) = -4/3$ and the amplitude is independent of the fermion mass. Therefore, if we combine two $gg \rightarrow h$ amplitudes, *both* coming from fermions far heavier than the Higgs mass, the net amplitude also insensitive to the individual fermion masses and only depends on the strength of the Higgs-fermion couplings:

$$A_t(gg \rightarrow h) + A_T(gg \rightarrow h)|_{m_h \ll 2m_t, 2M_T} = \frac{\alpha_s m_H^2}{4\pi v} \left(-\frac{4}{3} \right) (\kappa_t + \kappa_T). \quad (2.5)$$

Plugging in the couplings in in Eq. (2.2), we find the $gg \rightarrow h$ amplitude is independent of the mixing between the top and top-partner up to corrections of $\mathcal{O}\left(\frac{m_H^2}{4m_t^2}\right)$.

A crucial requirement for this insensitivity is that both fermions are heavy compared to the external momenta. This requirement teaches us two things. First, it tells us that this insensitivity of $gg \rightarrow h$ to SM fermion - new fermion mixing is only possible for the top sector; all other quarks are light compared to m_H^2 so Eq. (2.5) no longer holds¹. Second, being a $2 \rightarrow 1$ process, the total invariant mass entering the loop (\hat{s}) in $gg \rightarrow h$ is fixed to m_H^2 . However, this is not true for more general processes, such as when the Higgs recoils against other final state particles; there, $\hat{s} \gg m_H^2$ is possible. We emphasize that, to guarantee $\hat{s} \gg m_H^2$, one must focus on Higgs production with lots of recoil. Once higher-order corrections to $gg \rightarrow h$ [15–18] are taken into account, the Higgs will acquire some recoil. However, inclusive $pp \rightarrow h + X$ is dominated by $p_T \lesssim m_H$, which is insufficient to unveil the properties of the internal fermion loop. We must instead look to Higgses produced in association with one or more high- p_T objects.

2.2 Low energy Higgs theorems and the insensitivity of the hgg coupling

In this section we describe how a low energy theorem is responsible for the insensitivity of the dimension-five coupling hgg .

Consider a colored fermionic particle which transforms under the fundamental of $SU(3)_c$, and whose mass comes at least partially from electroweak symmetry breaking, $M = M(H)$. In this case, it is well known [19, 20] that the effect of this particle in the hgg coupling at low energies ($E \ll M$) would be described by

$$\mathcal{L}_{h^2 gg} = \frac{g_s^2}{96\pi^2} G_{\mu\nu}^a G^{a\mu\nu} \left(A_1 h + \frac{1}{2} A_2 h^2 + \dots \right), \quad (2.6)$$

¹See Ref. [14] for constraints on light fermion-new fermion mixing coming from this breakdown.

where the coefficients A_n can be written as

$$A_n \equiv \frac{\partial^n}{\partial H^n} \ln \det \mathcal{M}^\dagger \mathcal{M}(H)|_{h \rightarrow v} , \quad (2.7)$$

H is the Higgs doublet, and \mathcal{M} is the heavy fermion mass matrix.

In Composite Higgs and in Little Higgs models, the Higgs is a pseudo-Goldstone boson. This property restricts the coupling of the Higgs to fermions, hence the form of \mathcal{M} . In these models, the form of the mass matrix factorizes as follows

$$\det \mathcal{M}^\dagger \mathcal{M}(H) = \rho(H/f) \times \rho'(\text{couplings, masses}) \quad (2.8)$$

where f is the scale at which the global symmetry is broken, resulting in the appearance of the pseudo-Goldstone boson sector. For example, in the minimal Composite Higgs (i.e. coset $SO(5)/SO(4)$), $\rho = \sin^2(2H/f)$. This is similar to the fact that the pion non-derivative interactions appear as a function of the spurion π/f_π . As a result of this restriction, when one evaluates the effect of the fermion sector on the hgg coupling, the dependence in the coupling and mass (i.e. the dependence in the piece ρ' in Eq. 2.8) factors out and one is left with

$$\frac{\partial}{\partial H} \ln \det \mathcal{M}^\dagger \mathcal{M}(H)|_{h \rightarrow v} = \frac{\partial}{\partial H} \ln \rho(H/f)|_{h \rightarrow v} \quad (2.9)$$

which is just a function of the parameter

$$\xi = \frac{v^2}{f^2} . \quad (2.10)$$

All dependence on the coupling and mass of the top-partners disappears in the low energy limit. This statement goes beyond the leading $m \rightarrow \infty$ terms calculated in in Eq. (2.5). It tells us that even when higher order $1/m$ terms are taken into account, the hgg coupling in CH and LH models will only depend on ξ .

From the point of view of the effective theory, the inclusion of a hard jet in the final state corresponds to adding higher dimension operators. At the level of processes with one extra gluon, one needs to consider three dimension-seven operators [21] (i.e. dimension-eight operators with one v -insertion), which have the form

$$h \left(c_1 D_\alpha G_{\mu\nu} D^\alpha G^{\mu\nu} + c_2 G_\nu^\mu G_\rho^\nu G_\mu^\rho + c_3 D^\mu G_{\mu\nu} D_\alpha G^{\alpha\nu} \right) . \quad (2.11)$$

As we will see in the next Sec. 4, the effect of top-partners in the processes involving those operators does carry information about the coupling and masses of the top-partners.

3 Top-partners in pseudo-Goldstone Higgs models

In models where the Higgs is a pseudo-Goldstone boson and assuming only one top-partner, the coupling of the top ($t_{L,R}$) and top-partner ($T_{L,R}$) mass eigenstates to the Higgs can be written in terms of field-dependent masses:

$$- \mathcal{L}_m = m_t(h) \bar{t}_R t_L + M_T(h) \bar{T}_R T_L + \text{h.c.} \quad (3.1)$$

where, at lowest order in the strong scale f , $m_t(h)$ and $M_T(h)$ can be parametrized as [22]

$$m_t(h) = \frac{y_t h}{\sqrt{2}} \left(1 - \frac{c_t}{2} \frac{h^2}{f^2} \right), \quad M_T(h) = \lambda_T f \left(1 + a_T \frac{h^2}{f^2} \right), \quad (3.2)$$

with $a_T = \mathcal{O}(y_t^2/\lambda_T^2)$. The constant $c_t = 2a_T + c_\sigma$, where c_σ is a contribution coming from the non-linearity of the Higgs in pseudo-Goldstone models; this piece is model dependent, but $\mathcal{O}(y_t^2/f^2)$. Expanding $h \rightarrow v + h$ and continuing to work to lowest order in $\xi = v^2/f^2$, the Higgs couplings in Eq. (3.2) can be massaged into the same form as Eq. (2.2):

$$h \bar{t} t : \frac{m_t}{v} (1 - 2a_T \xi + \mathcal{O}(\xi^2)), \quad h \bar{T} T : \frac{M_T}{v} (2a_T \xi + \mathcal{O}(\xi^2)), \quad (3.3)$$

Therefore, we can identify

$$\sin^2(\theta_R) = 2a_T \xi + \mathcal{O}(\xi^2), \quad (3.4)$$

where the $\mathcal{O}(\xi^2)$ correction includes the non-linear piece c_σ .

Despite the fact that CH and LH models come in many varieties and have various field content and underlying symmetry, the mass matrices for the top-partner sector – at least for several well-studied models – can all be cast in the form Eq. (2.1) up to terms of order $\mathcal{O}(1/f^2)$. This mapping is shown explicitly in Appendix A. Following the steps in Eq. (3.2 - 3.4) for a given CH or LH model, we find

$$a_T = \frac{c^2 y_t^2}{\lambda_T^2}, \quad (3.5)$$

where c is an order one coefficient arising from the linear coupling of elementary and composite fermions. Different CH, LH models yield different c . For example, $c = 1$ in the littlest Higgs model. In Fig. 2 we show the relation between the mixing angle and the parameters in the parametrization in Eq. (3.2). Large values of $\sin^2(\theta_R)$ imply low values of the scale of breaking of the global symmetry or large coupling a_T , i.e. $\lambda_T \simeq y_t$.

3.1 Current bounds

The scale of breaking f depends on the UV completion of the theory. This scale is subject to electroweak precision tests [23] and flavor constraints, which depend on the assumptions on the symmetry structure and spectrum of the theory. For example, one could imagine that the UV completion preserves custodial symmetry [24], or that there is a spectrum designed to minimize the S parameter [25]. One could also assume there is a specific flavor structure [26] in the model at the scale f which keeps the flavor constraints under control. Regardless of these UV-sensitive issues, we expect modifications on the way the Higgs realizes electroweak symmetry breaking, hence modifications on the Higgs couplings to SM fields. Keeping an open mind about the UV structure of the top-partner theories, we will consider $\xi \lesssim 0.3$, the current bounds from Higgs signal-strength fits [27] (though the actual bound on ξ depends on the specific model). In practice, the parameter $\sin^2(\theta_R)$ is more convenient to use than a_T and ξ . Motivated by the bounds on ξ and the expression for a_T (Eq. (3.5)), we consider $\sin^2(\theta_R) \leq 0.4$ in all numerical studies.

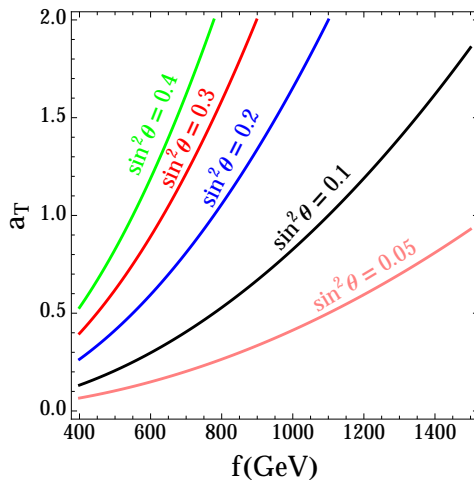


Figure 2. Lines with constant mixing angle $\sin^2(\theta_R)$ in the (f, a_T) plane.

Searches for top-partners in pair production through color processes, i.e. $pp \rightarrow T\bar{T}$ compete with the search we propose here, but the comparison would depend on the electroweak quantum numbers, e.g. the left and right handed composition [10] and what they decay to. The phenomenology could be driven by leptonic channels [28] or more complicated multijet or boosted signatures [29, 30]. Similarly, single production of the top-partner depends on the flavor structure of the model and how electroweak precision is addressed [29, 31].

4 The process $pp \rightarrow H + j$

Having mapped the top-mixing sector of CH and LH models into our parameterization, we are ready to explore the effects of top-partners on Higgs plus jet production. We start by looking at some limiting cases, then give numerical results both at parton level and after including the parton distribution functions (PDFs)².

4.1 Generalities

When the Higgs is produced in association with a jet, the assumptions of the low-energy theorem no longer holds. Specifically, for a given $p_{T,h} = p_{T,j}$, there is a bound on \hat{s} , $\hat{s} \geq 2p_T(p_T + \sqrt{m_H^2 + p_T^2})$. For sufficient p_T , this \hat{s} is no longer small compared to the mass of the fermion (top, or top-partner) running around the loop, we can no longer take the simple $\hat{s} \rightarrow 0$ limit and must retain the full dependence of the loop functions on \hat{s}/m_f^2 . To get some idea of how the $h + j$ cross section changes with \hat{s}/m_f^2 , we can look at the limiting cases: i.) high- p_T and ii.) low- p_T .

There are four partonic subprocess that contribute to $pp \rightarrow h + j$,

$$gg \rightarrow h + g, gq \rightarrow h + q, \bar{q}g \rightarrow h + \bar{q}, q\bar{q} \rightarrow h + g . \quad (4.1)$$

²For a very recent study of Higgs plus jets in the context of dimension-seven operators, see Ref. [32].

The actual breakdown of the subprocesses depends on p_T , the scale choice, and the PDFs, but gluon-gluon initiated subprocesses typically dominate, so we focus on $gg \rightarrow h+g$ for now. The $gg \rightarrow h+g$ cross section can be decomposed as a sum over the various gluon helicity configurations [33, 34] and the different fermions running in the loop:

$$\hat{\sigma}(gg \rightarrow gh) = \frac{\beta_H}{16\pi\hat{s}} \frac{\alpha_s^3}{4\pi v^2} \frac{3}{2} \left(\sum_{\lambda_i=\pm} \left| \sum_{f_i} \mathcal{M}_{\lambda_1\lambda_2\lambda_3}^i(\hat{s}, \hat{t}, \hat{u}, m_i, y_i) \right|^2 \right), \quad (4.2)$$

where β_H is the final state velocity, $\lambda_i = \pm$ are the helicities of the 3 gluons³, and f_i indicates the different fermion species running in the loop. For simplicity, when looking at the limiting cases, we will focus on one helicity configuration, \mathcal{M}_{+++} . We will also consider only one fermion species (mass m , Yukawa coupling $y = \frac{m}{v}\kappa$) running around the loop and take the center-of-mass rapidity (y^*) to be zero.

- In the high- p_T limit $p_T \gg m, m_H$, \mathcal{M}_{+++} contains single- and double-logarithms of the form [33, 34]

$$\mathcal{M}_{+++} \Big|_{p_T \gg m, m_H} \propto \frac{m^2 \kappa}{p_T} \left(A_0 + A_1 \ln \left(\frac{p_T^2}{m^2} \right) + A_2 \ln^2 \left(\frac{p_T^2}{m^2} \right) \right), \quad (4.3)$$

where A_0, A_1, A_2 are combinations of constants and m -independent logarithms such as $\ln \left(\frac{p_T}{m_H} \right)$ ⁴. The $A_{0,1,2}$ are complex, since the internal fermions can go on-shell if the momenta entering the loop are sufficiently large. In the high- p_T limit, the matrix element \mathcal{M}_{+++} clearly depends on both the mass and the Higgs coupling of the fermion in the loop. Note that \mathcal{M}_{+++} has positive mass dimension since we have pulled out the factor of v from the Yukawa coupling into the constant in front of Eq. (4.2).

- For low p_T , there is no dependence on the fermion mass since we are back in the $gg \rightarrow h$ limit of Sec. 2.2. Instead:

$$\mathcal{M}_{+++} \Big|_{m \gg p_T} \propto \kappa p_T \quad (4.4)$$

Having shown the two kinematic limits, let's now consider the form of \mathcal{M}_{+++} when there are two contributions, one from a lighter (EW-scale) fermion (i.e. the top quark, with mass m_t , coupling κ_{tt}) and one from a heavier, TeV-scale fermion (the top-partner, mass M_T , coupling κ_{TT}). When the final state has low- p_T , the Higgs is approximately at rest, and the low-energy theorem applies. Raising the p_T , we enter an intermediate regime where the $p_T \gtrsim O(m_t)$ but $p_T \ll M_T$. Approximating the top and top-partner contributions with the high- p_T and low- p_T limits, respectively, the matrix element in this regime is (schematically, and up to higher order corrections):

$$\mathcal{M}_{+++} \Big|_{m_t \ll p_T \ll M_T} \propto \frac{m_t^2 \kappa_t}{p_T} \left(A_{t,0} + A_{t,1} \ln \left(\frac{p_T^2}{m_t^2} \right) + A_{t,2} \ln^2 \left(\frac{p_T^2}{m_t^2} \right) \right) + \kappa_T p_T. \quad (4.5)$$

³Here we use the same convention as [34], namely that all momenta are outgoing.

⁴Relaxing the assumption of $y^* = 0$, these coefficients will depend on the center-of-mass rapidity as well.

We see that the top-partner leads to a term in the amplitude proportional to p_T . This linear term will lead to a slower dropoff in the cross section as we push to higher p_T . The matrix element in this kinematic region is sensitive to the top mass and Yukawa, and the top-partner Yukawa. There is no dependence on the top-partner mass until we go to an even higher p_T regime, $p_T \gg m_t, m_H, M_T$. There,

$$\begin{aligned} \mathcal{M}_{+++} \Big|_{m_t \ll p_T \ll M_T} &\propto \frac{m_t^2 \kappa_t}{p_T} \left(A_{t,0} + A_{t,1} \ln \left(\frac{p_T^2}{m_t^2} \right) + A_{t,2} \ln^2 \left(\frac{p_T^2}{m_t^2} \right) \right) \\ &+ \frac{M_T^2 \kappa_T}{p_T} \left(A_{T,0} + A_{T,1} \ln \left(\frac{p_T^2}{M_T^2} \right) + A_{T,2} \ln^2 \left(\frac{p_T^2}{M_T^2} \right) \right). \end{aligned} \quad (4.6)$$

4.2 Matrix Element level

We now turn to numerics to study how the matrix elements change in a top-partner setup as the final state p_T is increased. Since gg is the dominant contribution to the total cross section, let us continue to focus on $gg \rightarrow h + g$. A useful variable is the ratio of partonic matrix elements squared:

$$\frac{\left| \sum_{\lambda_i=\pm} \mathcal{M}_{t+T} \right|^2}{\left| \sum_{\lambda_i=\pm} \mathcal{M}_{SM} \right|^2} = \frac{\left| \sum_{\lambda_i=\pm} \left(M_{\lambda_1 \lambda_2 \lambda_3}(\hat{s}, \hat{t}, \hat{u}, m_t, \kappa_t) + M_{\lambda_1 \lambda_2 \lambda_3}(\hat{s}, \hat{t}, \hat{u}, M_T, \kappa_T) \right) \right|^2}{\left| \sum_{\lambda_i=\pm} M_{\lambda_1 \lambda_2 \lambda_3}(\hat{s}, \hat{t}, \hat{u}, m_t, 1) \right|^2}. \quad (4.7)$$

The Mandelstam variables depend on m_H , the p_T of the Higgs (or the recoiling jet) and the rapidity of the center-of-mass frame, y^* . For a given p_T , the minimum \hat{s} occurs when $y^* = 0$. As $\hat{s} = 2 p_T (\sqrt{p_T^2 + m_H^2} + p_T) + m_H^2$, $\hat{t} = \hat{u} = (m_H^2 - \hat{s})/2$, in this kinematic region Eq. (4.7) is a function of p_T , the heavy fermion mass M_T , and the mixing angle θ_R . Fixing M_T to three different values, the ratio of partonic matrix-elements squared is shown in Fig. 3 as a function of $\sin^2(\theta_R)$ and p_T . The shapes of the contours in Fig. 3 can be understood by the different functional forms of Eq. (4.5) and Eq. (4.6): for $p_T \lesssim M_T$ (below the red dashed line) the ratios have a similar shape for all three M_T values, while for $p_T \gtrsim M_T$ the contours change shape and their values depend on the M_T assumed. Large ratios $\sim O(5)$ are possible, however the largest differences come at high- p_T where the cross section is smallest. To gauge the effect on the full cross section we need to fold in parton distribution functions.

4.3 Including the effect of PDFs and running

We now move onto the effect of including scale and PDF effects. This has been done by adapting Herwig [35] amplitudes to include contributions from a top-partner. The modified matrix elements were then interfaced with HOPPET [36] and LHAPDF [37] to generate the distributions. We also implemented the top-partner in MCFM [38] to check our results⁵. For the SM, our calculation includes the effects of both the bottom and top quarks; for the top-partner scenarios we include the top, top-partner (with θ_R dependent Yukawa couplings),

⁵Finite-mass effects in loops are implemented also in Pythia [39], POWHEG [40] or MC@NLO [41], so we could have used any of those programs instead of Herwig.

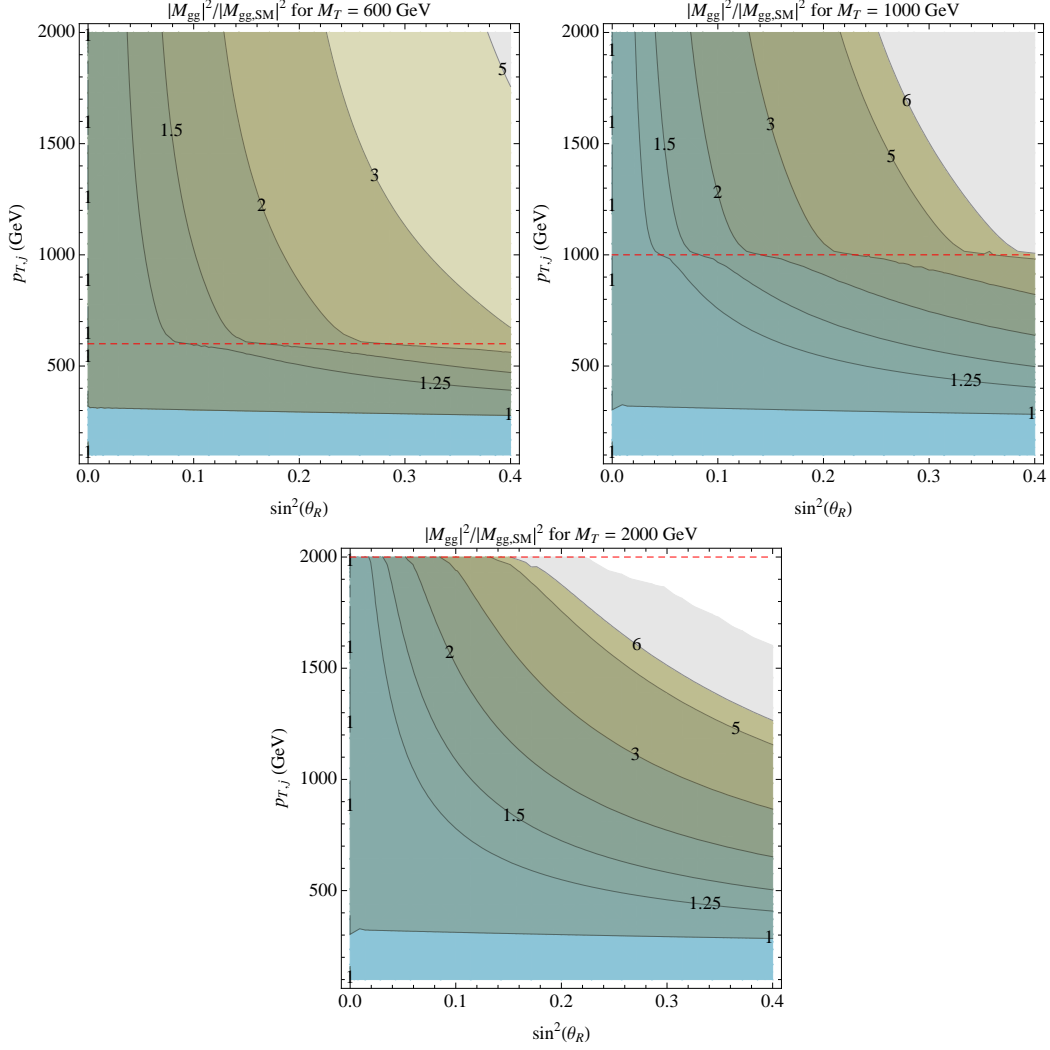


Figure 3. Ratio of partonic $gg \rightarrow h + g$ matrix elements squared in a theory with a 600 GeV (top left), 1 TeV (top right) and 2 TeV (bottom) top-partner, compared to the SM value. The ratio is a function of top-mixing angle, and the p_T and y^* of the final state. Projecting onto $y^* = 0$ (the minimum $\sqrt{\hat{s}}$ for a given p_T), the ratio is a function of the mixing angle and p_T alone. The matrix elements include all gluon polarizations. The dashed red line indicates where $p_{T,j} = M_T$.

and bottom quark contributions. The differential p_T distribution is shown below in Fig. 4 for the SM and six top-partner scenarios – three different M_T values and two different $\sin^2(\theta_R)$ values. This plot exhibits the same features we saw at the partonic level, though diluted by the PDFs. First, as dictated by the low-energy theorem, all top-partner scenarios converge to the SM result at low- p_T . Second, as suggested by the analytic results in Sec. 4.1, the p_T -spectra in top-partner scenarios is harder than the SM. Finally, the spectra for a given mixing angle are not sensitive to the top-partner mass until the final state $p_T \sim M_T$.

The difference in the p_T spectrum between the SM and a theory with a top-partner is our main result. The full p_T spectrum is, however, an experimentally difficult quantity to measure since the higher p_T bins will suffer from low statistics. A similar, though perhaps

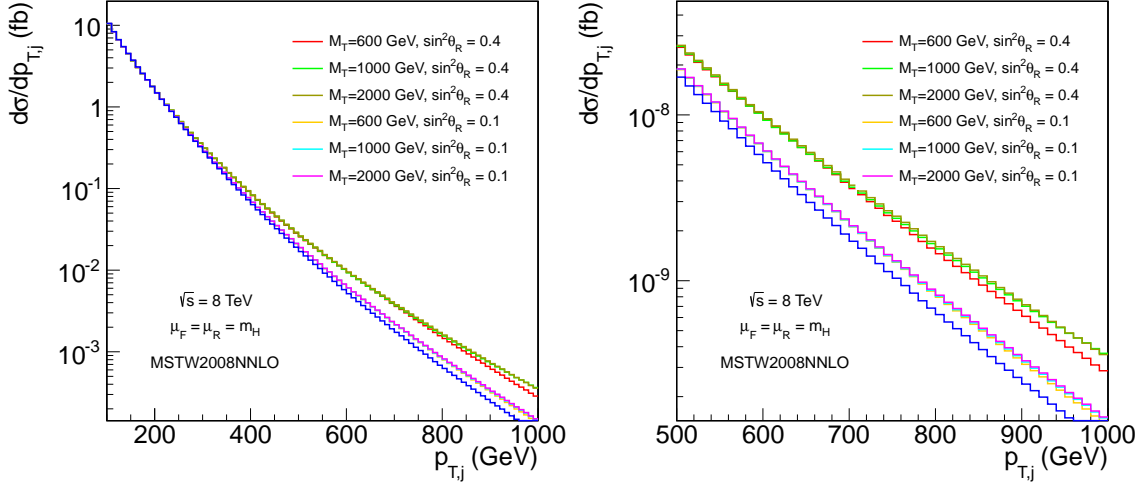


Figure 4. (Left panel) differential cross section $d\sigma/dp_T$ at a $\sqrt{s} = 8$ TeV LHC for the SM (top and bottom quarks) in blue, and including a top-partner. Three different top-partner masses are shown, 600 GeV, 1 TeV and 2 TeV and two different top-mixing angles $\sin^2(\theta_R) = 0.1, 0.4$. (Right panel) same spectra, zoomed in to the high- p_T range 500 GeV – 1 TeV.

experimentally more tractable observable is the net Higgs plus jet cross section for all events that satisfy a given p_T cut, i.e.

$$\sigma(p_T > p_T^{\text{cut}}) = \int_{p_T^{\text{cut}}} dp_T \frac{d\sigma}{dp_T}. \quad (4.8)$$

Using $\sigma(p_T > p_T^{\text{cut}})$, we define a new variable δ ,

$$\delta(p_T^{\text{cut}}, M_T, \sin \theta) = \frac{\sigma_{t+T}(p_T > p_T^{\text{cut}}, \mu, M_T, \sin \theta) - \sigma_t(p_T > p_T^{\text{cut}}, \mu)}{\sigma_t(p_T > p_T^{\text{cut}}, \mu)}. \quad (4.9)$$

which encapsulates the effect of a top-partner in the cross section. Here, σ_{t+T} is the cross-section in a theory with a top-partner of a given mass and mixing angle, while σ_t is the cross-section for the SM. In Fig. 5 we show the value of δ as a function of p_T^{cut} for different values of M_T and the mixing angle. Obviously, the effect increases with the top-mixing angle. As in the differential distributions, heavier top-partners lead to a harder p_T spectrum, but the effect δ is negligible until $p_T > M_T$. To generate this plot, we have taken $\mu_R = \mu_F = \mu = \frac{1}{2}(p_T + \sqrt{p_T^2 + m_h^2})$ and $\sqrt{s} = 8$ TeV.

While gluon-initiated subprocess dominate $pp \rightarrow h + j$ for low p_T , it is interesting to see how the breakdown of the cross section into partonic subprocesses changes as we increase the p_T . In Fig. 6 we plot the ratio

$$\frac{d\sigma_i}{dp_T} / \frac{d\sigma_{\text{tot}}}{dp_T}, \quad i = gg, gq + \bar{q}g, \text{ or } q\bar{q} \quad (4.10)$$

in the SM and in the theory with a 1 TeV top-partner (here, $\frac{d\sigma_{\text{tot}}}{dp_T}$ is the differential distribution including all channels in the respective theory). The dominant cross section

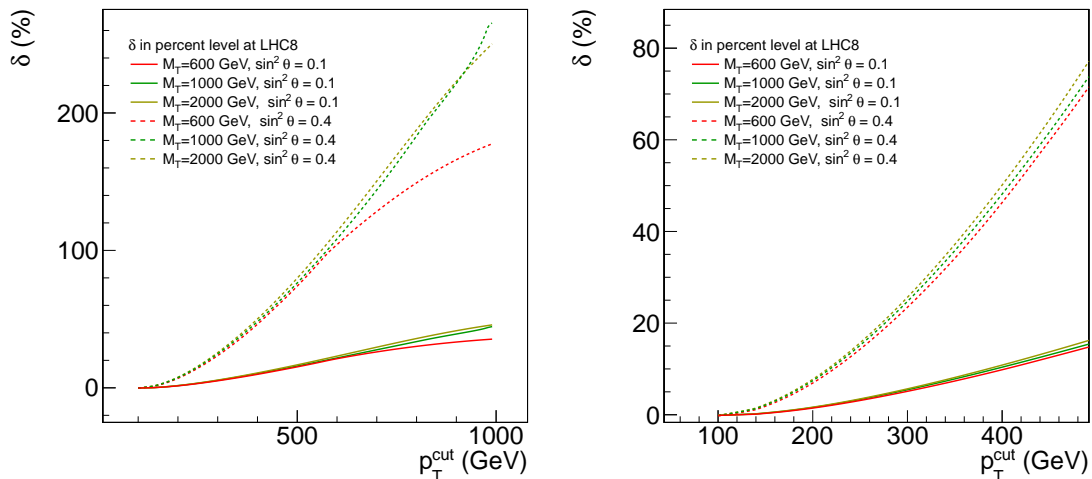


Figure 5. (Left panel) δ as a function of p_T^{cut} for different values of M_T and the mixing angle. (Right panel) A zoom in the interesting range of p_T . These plots have been generated with $\mu = \frac{1}{2}(p_T + \sqrt{p_T^2 + m_h^2})$ and a $\sqrt{s} = 8$ TeV LHC.

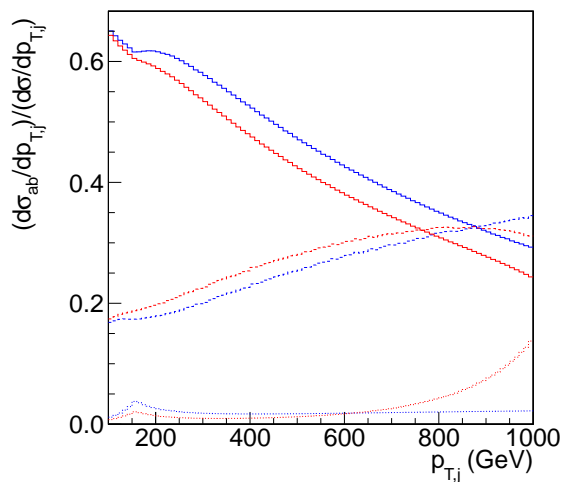


Figure 6. Breakdown of the differential cross section $d\sigma/dp_T$ into different initial state channels, $d\sigma_i/dp_T$, where $i = gg$ (solid), $qg + \bar{q}g$ (dashed) and $q\bar{q}$ (dotted). The blue (red) lines correspond to the SM (top-partner) theory. The top-partner in this plot corresponds to $M_T = 1$ TeV and $\sin^2(\theta_R) = 0.4$. The contribution from $qg + \bar{q}g$ is not shown (thus the sum does not equal 1.0) since it is identical to $qg + \bar{q}g$.

corresponds to gg for jet $p_T \lesssim 800$ GeV, after which qg becomes the dominant subprocess. The crossover is delayed in the case of a theory with a top-partner respect to the SM, as the former exhibits a harder spectrum. Note also that the qg and $q\bar{q}$ initial states do depend on the quark mass. For example, in the right-hand diagram in Fig. 1, the dependence on the quark in the loop can be understood as the t -channel gluon virtuality enhancing the

double-logarithmic structure in the matrix element. The sharp features in the $\bar{q}q$ subprocess at $p_T \sim m_T$ and $p_T \sim M_T$ come from a resonant enhancement in the loop functions near $\hat{s} \sim 4p_T^2 \sim 4m_t^2$ or $\hat{s} \sim 4M_T^2$ respectively. Had we plotted to $p_T > 1$ TeV, the $\bar{q}q$ fraction in the top-partner scenario would shrink again.

Although we have calculated loops of top quarks and top-partners, our $pp \rightarrow h + j$ calculation is still a lowest-order calculation. Being a lowest order (LO) result – especially given that the cross section depends on α_s^3 – one immediate worry is that our result may be highly dependent on the scale choice and the choice of PDF. However, provided we look at a ratio of cross sections, such as $\delta(p_T^{\text{cut}})$, one might expect most dependence on these input choices should drop out. We have confirmed this intuition with cross-checks. First, calculating $\delta(p_T^{\text{cut}})$ for three different values of the factorization and renormalization scheme, $\mu_R = \mu_F = \mu = \left(p_T + \sqrt{p_T^2 + m_h^2}\right)/2$, $\sqrt{p_T^2 + m_h^2}$ and m_H , we find the difference in the ratio between the three schemes, i.e. $\delta(p_T^{\text{cut}}, \mu)/\delta(p_T^{\text{cut}}, \mu')$ is below the percent level. Next, we verified the stability of $\delta(p_T^{\text{cut}})$ under changes in the PDF schemes by comparing $\delta(p_T^{\text{cut}})$ calculated with two different PDF sets. Using top-partner parameters $M_T = 1$ TeV, $\sin^2(\theta_R) = 0.4$, the ratio of $\delta(p_T^{\text{cut}})$ calculated with MSTW2008nlo68c1 PDFs [42] to $\delta(p_T^{\text{cut}})$ calculated using cteq6mE [43] is shown below in Fig. 7. The effect is less than 2% in the range of p_T we will consider.

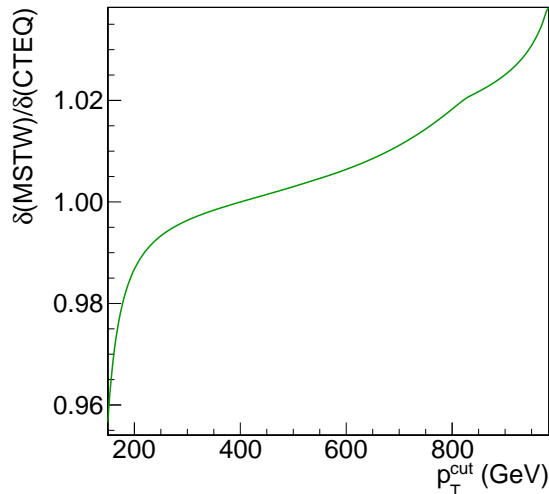


Figure 7. The ratio of $\delta(p_T^{\text{cut}})$ calculated with MSTW2008nlo68c1 parton distribution functions to $\delta(p_T)$ calculated with cteq6mE. The top-partner used for calculating $\delta(p_T)$ has mass 1 TeV and mixing angle $\sin^2(\theta_R) = 0.4$. All distributions were generated using 8 TeV LHC parameters.

We move on to study the effect of the collider energy by comparing the results for $\sqrt{s} = 8$ TeV and $\sqrt{s} = 14$ TeV. The quantity $\delta(p_T^{\text{cut}})$ is shown in Fig. 8. Comparing with the same quantity at $\sqrt{s} = 8$ TeV Fig. 5, one can see that the ratio does not depend strongly on the energy of the collider.

Finally, a comment on the dependence of the result on the rapidity acceptance for the

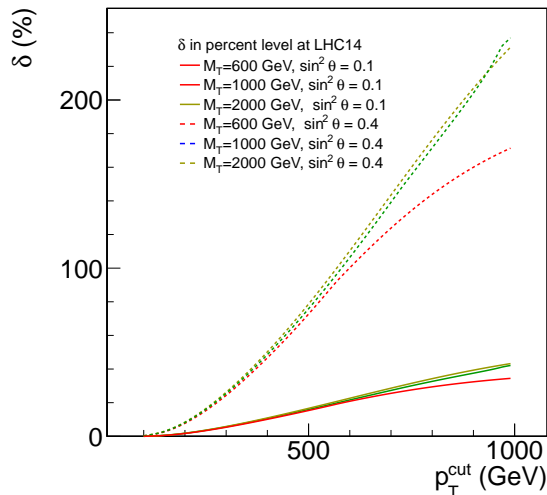


Figure 8. δ as a function of p_T^{cut} for different values of M_T and the mixing angle for $\sqrt{s} = 14$ TeV.

jet. The topology we are looking at, with a Higgs recoiling against a high- p_T jet tends to produce very central events. This is just because at high p_T there is not enough phase space to produce high rapidity jets. Indeed, our Herwig implementation, in which we have integrated over all rapidities, is in agreement with MCFM with a cut $|\eta| < 5$. We have checked in MCFM that moving the cut on jet rapidity from $|\eta| < 5$ to $|\eta| < 2.5$, which corresponds to the acceptance of the CMS and ATLAS central trackers, does not alter our results.

5 Stability against higher order corrections and experimental uncertainties

In Sec. 4 we discussed the stability of the results when changing the renormalization scale and PDF sets, finding that the effect is at the percent level. In this section we will focus on the effect of adding higher order corrections and experimental uncertainties.

Currently, there is no available computation of Higgs plus jet at next-to-leading order (NLO) including finite mass effects⁶. This calculation is beyond the scope of this paper, but given its importance for constraining new physics, one would hope that it becomes available in the near future. Given this situation, the best one can do is to evaluate the NLO effects, differentially, in the infinite top mass limit. We have evaluated the K-factor, the LO and NLO Higgs plus jets using MCFM [38] in the infinite top mass limit in the differential distribution $d\sigma/dp_T$. The K-factor is rather flat (roughly $O(2)$) as a function of p_T for $\mu = \sqrt{p_T^2 + m_H^2}$, but has a slope for $\mu = m_H$.

We expect the higher order corrections to produce changes in shape once the finite mass effects are taken into account. Nevertheless, as our observable is an integrated cross

⁶In fact, there exists a calculation of Higgs plus one jet at NLO, but contains only top-mass effects in the heavy-top limit up to $1/m_t$ corrections, so it can be used only at moderately low p_T [44].

section, dominated by the region near the p_T cut, we expect higher-order corrections to just amount to an overall K-factor, although this expectation should be corroborated with a explicit calculation. Moreover, one should aim to obtain as much information as possible from the *differential* cross section, whereas in this paper we have to limit ourselves to an integrated cross section with a p_T cut. With a NLO calculation with finite mass effects, the differential distribution would become a more powerful tool to disentangle new physics.

The most important experimental uncertainty for our observable would be energy and momentum smearing of the Higgs or the recoil jet. As we are using integrated cross sections as in Eq. (4.8), the effect of smearing would affect the region near the cut. Similarly, the effect of the underlying event would also produce some momentum smearing, although we expect it would be negligible at $p_T > 100$ GeV [45]. Therefore, at least for p_T cuts greater than ~ 200 GeV, we believe experimental effects should be small and will affect the SM and top-partner scenarios in a similar way.

6 Mass limits on top-partners

In this section we study the sensitivity of the 14 TeV LHC to the top-partner mass and coupling. The events we are focusing on are characterized by a high- p_T jet plus a Higgs boson.

Given a particular Higgs plus jet final state and some amount of luminosity, we can set limits on the top partners by comparing two hypothesis: SM Higgs plus jet production vs. Higgs plus jet production in a top partner scenario, where the latter hypothesis is a function of M_T and $\sin^2(\theta_R)$. For simplicity, and since there is no dedicated CMS/ATLAS search in Higgs plus hard jet to work off of, we will quantify the difference between the two hypothesis with the variable

$$\text{Significance} = \frac{S}{\sqrt{S_0}}, \quad (6.1)$$

where S is the signal

$$S = (\sigma_{t+T}(p_T > p_T^{\text{cut}}) - \sigma_t(p_T > p_T^{\text{cut}})) \times \mathcal{L}, \quad (6.2)$$

and S_0 is the SM piece, $S_0 = \sigma_t(p_T > p_T^{\text{cut}}) \times \mathcal{L}$. We claim sensitivity to rule out a top-partner at the 95 % confidence level if $S/\sqrt{S_0}$ at luminosity \mathcal{L} is bigger than 2.0.

This test statistics is only approximate as it assumes that the SM background can be completely removed. This is a reasonable assumption in the clean leptonic and photon final states. For the higher rate, hadronic Higgs decay modes the SM background is more problematic, though the requirement of a hard jet in the event is a useful handle for suppressing background. Dedicated studies of the backgrounds in all Higgs final states for Higgs plus hard jet events are well motivated, but beyond the scope of this paper.

Our test statistics also assumes that the cut efficiency for the SM and new physics Higgs plus jet events is the same, and that the Higgs branching ratios are not modified by new physics⁷. A final caveat in our significance measure is that we use LO cross sections

⁷As long as the top-partner is beyond threshold, the possible modification of Higgs branching ratios from the SM is a question which does not directly depend on the top-partner.

only. As we mentioned in Sec. 5, the complete, mass-dependent higher order corrections are not known yet and may carry some non-trivial fermion mass and p_T dependence.

In Fig. 9, we show the significance as a function of the mixing angle for a standard luminosity fo 300 fb^{-1} . With mixing angles $\sin^2(\theta_R) \gtrsim 0.05$, one would have sensitivity in a range from around 300 GeV to above 2 TeV. Recall that in Fig. 2 we showed the translation

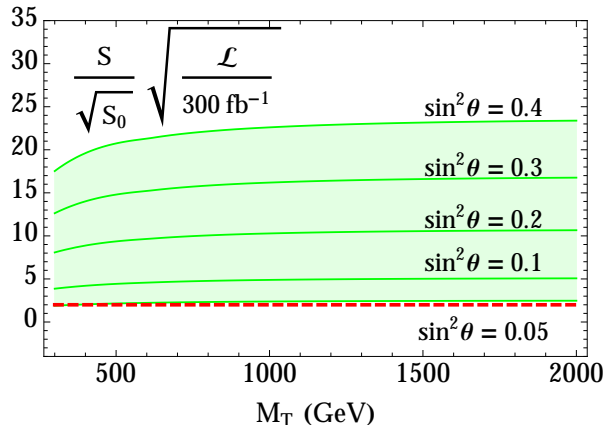


Figure 9. Significance as a function of the mixing angle for a standard luminosity fo 300 fb^{-1} .

between the mixing angle and the top-partner parametrizations in the literature. A limit of $\sin^2(\theta_R)$ at 0.05, is equivalent to a limit on the scale of breaking f for a fixed value of a_T . For example,

$$\sin^2(\theta_R) < 0.05 \Rightarrow f > 1.6 \text{ TeV, for } \lambda_T \simeq y_t . \quad (6.3)$$

In Sec. 4.3, we showed that $\delta(p_T^{\text{cut}})$ is very stable against changes in definitions of renormalization scale and PDF sets. We have checked that the quantity $S/\sqrt{S_0}$ is also rather stable. To do so, we define

$$\Delta(\omega_1, \omega_2) = \frac{S/\sqrt{S_0}(\omega_1) - S/\sqrt{S_0}(\omega_2)}{S/\sqrt{S_0}(\omega_1) + S/\sqrt{S_0}(\omega_2)}, \quad (6.4)$$

where ω_i is a label for the choice of running parameters. The value of Δ for the same two choices of PDF schemes mentioned in Sec. 4.3 is shown below in Fig. 10. As before, the effect at the sub-percent level. We have also checked agains changes in renormalization scales and PDF sets within a PDF scheme.

From Fig. 9, we see that the sensitivity curves are fairly flat, indicating that the $S/\sqrt{S_0}$ is mainly sensitive to the coupling. To see the difference between higher top-partner masses, we would need to look at higher- p_T , where there is simply not enough rate at $\sqrt{s} = 14 \text{ TeV}$. This fact makes the Higgs plus jet search quite complementary to traditional $pp \rightarrow T\bar{T}$ top-partner searches, where the production the rate is set by M_T alone. The decay of top-partners is more model dependent. However, at least in simple setups, the decay is completely governed by "Goldstone-equivalence" and is thus independent of the $T\bar{T}h$ coupling.

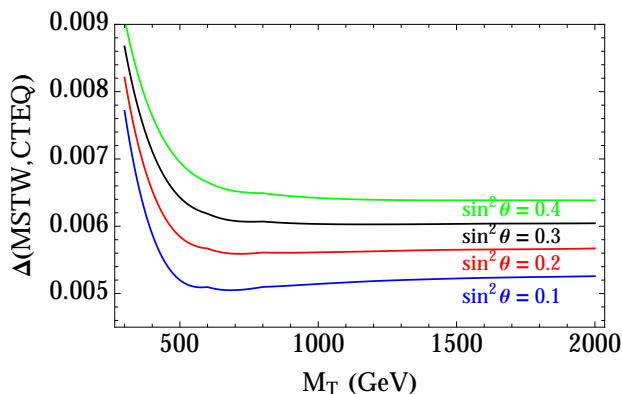


Figure 10. Δ for two choices of PDF schemes with a cut on $p_T > 200$ GeV.

As the sensitivity is rather flat with M_T for $M_T \simeq 600$ GeV, one can plot the luminosity required to set an exclusion as a function of the top-mixing angle alone. This is shown in the left panel of Fig. 11, where we have chosen a cut on p_T of 200 GeV. In the right panel of Fig. 11 we show the effect of changing this cut for $\sin^2(\theta_R) = 0.2$. As the cut increases, the sensitivity does increase until at about $p_T \simeq 400$ GeV, the cut is too hard and the sensitivity starts decreasing.

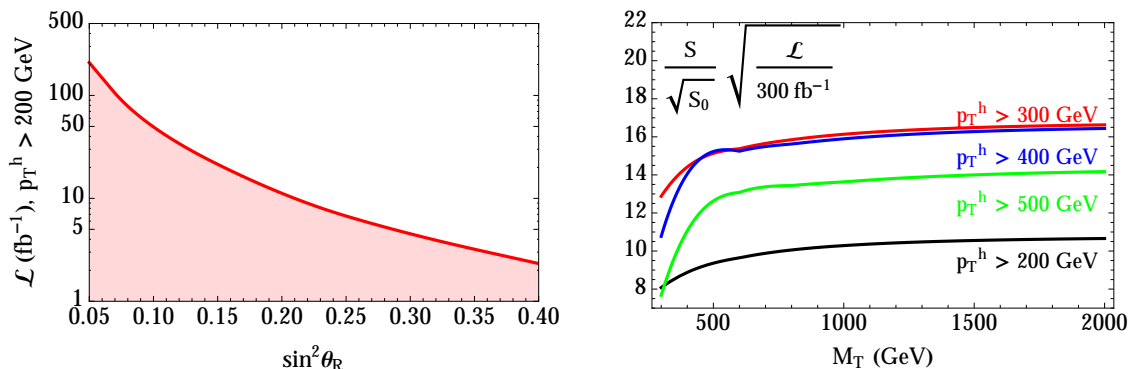


Figure 11. (Left panel) Luminosity (in fb^{-1}) required to rule out a mixing angle at the 2σ level with a cut on $p_T > 200$ GeV. (Right panel) Effect of raising the p_T cut on the significance, for $\sin^2(\theta_R) = 0.2$.

7 Conclusions

In this paper we have presented a first step to search for top-partners in events where the Higgs is produced in association with hard jets. This topology avoids the well-known low-energy cancellation acting on the hgg coupling when the Higgs is a pseudo-Goldstone boson that renders the $gg \rightarrow h$ process insensitive to the mass and coupling of the top-partner.

Our analysis is motivated by these type of models, but it just relies on the presence of a top-partner with couplings to the Higgs coming from electroweak symmetry breaking⁸.

We have worked out the dependence of the spectrum on the top-partners using variables which are not directly the differential distribution, but integrated distributions with a cut on p_T . We checked that the results at leading order are stable against choices of renormalization scales and PDF sets. We discussed what would be the effect of including NLO corrections. Unfortunately, no NLO computation is available in the finite mass limit. We did check that in the infinite mass limit the K-factor on the differential distribution is flat for appropriate choices of the renormalization scale.

Finally, we have assigned a significance for a top-partner signal, finding that 200 fb⁻¹ of data may access very low mixing angles $\sin^2(\theta_R) < 0.05$, for a large range of top-partner masses. These results are certainly encouraging and warrant more dedicated study.

Furthermore, more information could be obtained by looking at the differential distribution, as opposed to the integrated one. This study would require an excellent understanding of the NLO corrections of this distribution, a calculation we hope will become available in the near future.

Acknowledgements

The work of AB and VS is supported by the Science Technology and Facilities Council (STFC) under grant number ST/J000477/1.

A Choices in Model Space

Although our study would be model independent, one can map the parameter space of Composite and Little Higgs models into our setup. In particular, we show examples in the minimal coset $SO(5)/SO(4)$ [3] and study top-partners in the singlet and fundamental representation of $SO(4)$, which we denote by \mathbf{S} and \mathbf{F} . This includes the littlest Higgs models. As in Ref. [28], one can consider two choices for the representation of the operator which induces the mixing of the elementary fermions with the strong sector, namely $\mathbf{5}$ and $\mathbf{14}$ of $SO(5)$. We then end up with four different choices of representations, top-partners in the singlet ($\mathbf{S}_{\mathbf{5},\mathbf{14}}$) and fundamental ($\mathbf{F}_{\mathbf{5},\mathbf{14}}$) representations.

In Table 1, we show the translation between our parametrization and several benchmark models. Using

$$\xi = \frac{v^2}{f^2} = \sin^2 \epsilon. \quad (\text{A.1})$$

and $N = \sqrt{c_\epsilon^2 + c_{2\epsilon}^2}$,

⁸For instance, our result applies to extra dimensional models such as Ref. [46–50], and some topcolor models [51]

Model	m	Δ	M
S₅	$-\frac{cyf}{\sqrt{2}} \sin \epsilon$	$-\frac{yf}{\sqrt{2}} \sin \epsilon$	$-M_\Psi$
S₁₄	$-\frac{cyf}{2\sqrt{2}} \sin 2\epsilon$	$-\frac{yf}{2\sqrt{2}} \sin 2\epsilon$	$-M_\Psi$
F₅	$-\frac{cyf}{\sqrt{2}} \sin \epsilon$	$yf \sqrt{\cos^4 \frac{\epsilon}{2} + \sin^4 \frac{\epsilon}{2}}$	$-M_\Psi$
F₁₄	$-\frac{yf}{2\sqrt{2}} \sin 2\epsilon$	$\frac{yf}{2} \cos \epsilon N$	$-N^2 M_\Psi / 4$

Table 1. Translation between our parametrization and the choices in the model space.

References

- [1] H. Georgi and A. Pais, Phys. Rev. D **10**, 539 (1974). H. Georgi and A. Pais, Phys. Rev. D **12**, 508 (1975).
- [2] N. Arkani-Hamed, A. G. Cohen and H. Georgi, Phys. Lett. B **513**, 232 (2001) [arXiv:hep-ph/0105239]. N. Arkani-Hamed, A. G. Cohen, T. Gregoire and J. G. Wacker, JHEP **0208**, 020 (2002) [arXiv:hep-ph/0202089]. N. Arkani-Hamed, A. G. Cohen, E. Katz, A. E. Nelson, T. Gregoire and J. G. Wacker, JHEP **0208**, 021 (2002) [arXiv:hep-ph/0206020]. N. Arkani-Hamed, A. G. Cohen, E. Katz and A. E. Nelson, JHEP **0207**, 034 (2002) [arXiv:hep-ph/0206021]. T. Gregoire and J. G. Wacker, JHEP **0208**, 019 (2002) [arXiv:hep-ph/0206023]. I. Low, W. Skiba and D. Smith, Phys. Rev. D **66**, 072001 (2002) [arXiv:hep-ph/0207243]. M. Schmaltz, Nucl. Phys. Proc. Suppl. **117**, 40 (2003) [arXiv:hep-ph/0210415]. D. E. Kaplan and M. Schmaltz, JHEP **0310**, 039 (2003) [arXiv:hep-ph/0302049]. S. Chang and J. G. Wacker, Phys. Rev. D **69**, 035002 (2004) [arXiv:hep-ph/0303001]. W. Skiba and J. Terning, Phys. Rev. D **68**, 075001 (2003) [arXiv:hep-ph/0305302]. S. Chang, JHEP **0312**, 057 (2003) [arXiv:hep-ph/0306034]. H. C. Cheng and I. Low, JHEP **0309**, 051 (2003) [arXiv:hep-ph/0308199]. E. Katz, J. Y. Lee, A. E. Nelson and D. G. E. Walker, arXiv:hep-ph/0312287. A. Birkedal, Z. Chacko and M. K. Gaillard, JHEP **0410**, 036 (2004) [arXiv:hep-ph/0404197]. H. C. Cheng and I. Low, JHEP **0408**, 061 (2004) [arXiv:hep-ph/0405243]. D. E. Kaplan, M. Schmaltz and W. Skiba, Phys. Rev. D **70**, 075009 (2004) [arXiv:hep-ph/0405257]. M. Schmaltz, JHEP **0408**, 056 (2004) [arXiv:hep-ph/0407143]. I. Low, JHEP **0410**, 067 (2004) [arXiv:hep-ph/0409025]. K. Agashe, R. Contino and A. Pomarol, arXiv:hep-ph/0412089. P. Batra and D. E. Kaplan, arXiv:hep-ph/0412267. J. Thaler and I. Yavin, arXiv:hep-ph/0501036.
- [3] R. Contino, Y. Nomura and A. Pomarol, Nucl. Phys. B **671**, 148 (2003) [arXiv:hep-ph/0306259]. K. Agashe, R. Contino and A. Pomarol, Nucl. Phys. B **719**, 165 (2005) [arXiv:hep-ph/0412089]. R. Contino, L. Da Rold and A. Pomarol, Phys. Rev. D **75**, 055014 (2007) [arXiv:hep-ph/0612048]. A. Pomarol and F. Riva, JHEP **1208** (2012) 135 [arXiv:1205.6434 [hep-ph]]. D. Marzocca, M. Serone and J. Shu, JHEP **1208**, 013 (2012) [arXiv:1205.0770 [hep-ph]].
- [4] R. Contino, T. Kramer, M. Son and R. Sundrum, JHEP **0705**, 074 (2007) [hep-ph/0612180]. J. Mrazek, A. Pomarol, R. Rattazzi, M. Redi, J. Serra and A. Wulzer, Nucl. Phys. B **853**, 1 (2011) [arXiv:1105.5403 [hep-ph]]. G. F. Giudice, C. Grojean, A. Pomarol and R. Rattazzi, JHEP **0706**, 045 (2007) [hep-ph/0703164]. B. Keren-Zur, P. Lodone, M. Nardecchia, D. Pappadopulo, R. Rattazzi and L. Vecchi, Nucl. Phys. B **867**, 429 (2013) [arXiv:1205.5803 [hep-ph]]. F. Caracciolo, A. Parolini and M. Serone, JHEP **1302**, 066 (2013) [arXiv:1211.7290 [hep-ph]].

- [5] A. Falkowski, Phys. Rev. D **77**, 055018 (2008) [arXiv:0711.0828 [hep-ph]]. I. Low and A. Vichi, Phys. Rev. D **84**, 045019 (2011) [arXiv:1010.2753 [hep-ph]]. A. Azatov and J. Galloway, Phys. Rev. D **85**, 055013 (2012) [arXiv:1110.5646 [hep-ph]]. M. Montull, F. Riva, E. Salvioni and R. Torre, arXiv:1308.0559 [hep-ph].
- [6] E. Furlan, JHEP **1110**, 115 (2011) [arXiv:1106.4024 [hep-ph]].
- [7] A. Azatov, O. Bondu, A. Falkowski, M. Felcini, S. Gascon-Shotkin, D. K. Ghosh, G. Moreau and S. Sekmen, Phys. Rev. D **85**, 115022 (2012) [arXiv:1204.0455 [hep-ph]].
- [8] See for example, A. Falkowski, F. Riva and A. Urbano, arXiv:1303.1812 [hep-ph]. P. P. Giardino, K. Kannike, I. Masina, M. Raidal and A. Strumia, arXiv:1303.3570 [hep-ph].
- [9] R. Contino, C. Grojean, M. Moretti, F. Piccinini and R. Rattazzi, JHEP **1005**, 089 (2010) [arXiv:1002.1011 [hep-ph]].
- [10] See for example: CMS Collaboration, [CMS-PAS-B2G-12-012] and [CMS-PAS-B2G-12-015]. ATLAS Collaboration, [ATLAS-CONF-2013-060], [ATLAS-CONF-2013-056], [ATLAS-CONF-2013-018].
- [11] J. Kearney, A. Pierce and J. Thaler, arXiv:1306.4314 [hep-ph].
- [12] J. Kearney, J. Thaler and A. Pierce, arXiv:1304.4233 [hep-ph].
- [13] See for example, A. Djouadi, Phys. Rept. **457**, 1 (2008) [hep-ph/0503172].
- [14] C. Delaunay, C. Grojean and G. Perez, arXiv:1303.5701 [hep-ph].
- [15] A. Djouadi, M. Spira and P. M. Zerwas, Phys. Lett. B **264** (1991) 440.
- [16] R. V. Harlander and W. B. Kilgore, Phys. Rev. Lett. **88** (2002) 201801 [hep-ph/0201206].
- [17] C. Anastasiou, K. Melnikov, F. Petriello, Nucl. Phys. **B724** (2005) 197-246. [hep-ph/0501130].
- [18] S. Catani and M. Grazzini, Phys. Rev. Lett. **98** (2007) 222002 [hep-ph/0703012]; M. Grazzini, JHEP **0802** (2008) 043. [arXiv:0801.3232 [hep-ph]].
- [19] J. R. Ellis, M. K. Gaillard and D. V. Nanopoulos, Nucl. Phys. B **106** (1976) 292; M. A. Shifman, A. I. Vainshtein, M. B. Voloshin and V. I. Zakharov, Sov. J. Nucl. Phys. **30** (1979) 711 [Yad. Fiz. **30** (1979) 1368].
- [20] B. A. Kniehl and M. Spira, Z. Phys. C **69** (1995) 77 [arXiv:hep-ph/9505225].
- [21] J. A. Gracey, Nucl. Phys. B **634**, 192 (2002) [Erratum-ibid. B **696**, 295 (2004)] [hep-ph/0204266].
- [22] M. Gillioz, R. Grober, C. Grojean, M. Muhlleitner and E. Salvioni, JHEP **1210**, 004 (2012) [arXiv:1206.7120 [hep-ph]].
- [23] R. Contino, D. Marzocca, D. Pappadopulo and R. Rattazzi, JHEP **1110**, 081 (2011) [arXiv:1109.1570 [hep-ph]]. A. Pich, I. Rosell and J. J. Sanz-Cillero, Phys. Rev. Lett. **110**, 181801 (2013) [arXiv:1212.6769 [hep-ph]].
- [24] See for example, K. Agashe, A. Delgado, M. J. May and R. Sundrum, JHEP **0308**, 050 (2003) [hep-ph/0308036].
- [25] See for example, C. Csaki, C. Grojean, L. Pilo and J. Terning, Phys. Rev. Lett. **92**, 101802 (2004) [hep-ph/0308038]. J. Hirn and V. Sanz, Phys. Rev. Lett. **97**, 121803 (2006) [hep-ph/0606086]. J. Hirn, A. Martin and V. Sanz, JHEP **0805**, 084 (2008) [arXiv:0712.3783 [hep-ph]].

- [26] See for example, M. Redi and A. Weiler, JHEP **1111**, 108 (2011) [arXiv:1106.6357 [hep-ph]].
C. Csaki, A. Falkowski and A. Weiler, JHEP **0809**, 008 (2008) [arXiv:0804.1954 [hep-ph]].
C. Delaunay, O. Gedalia, S. J. Lee, G. Perez and E. Ponton, Phys. Rev. D **83**, 115003 (2011) [arXiv:1007.0243 [hep-ph]].
- [27] ATLAS Collaboration, [ATLAS-CONF-2013-034]. CMS Collaboration, [CMS-PAS-HIG-13-005].
- [28] A. De Simone, O. Matsedonskyi, R. Rattazzi and A. Wulzer, JHEP **1304**, 004 (2013) [arXiv:1211.5663 [hep-ph]].
- [29] M. Redi, V. Sanz, M. de Vries and A. Weiler, JHEP **08**, 008 (2013) [arXiv:1305.3818 [hep-ph]].
- [30] G. D. Kribs, A. Martin and T. S. Roy, Phys. Rev. D **84**, 095024 (2011) [arXiv:1012.2866 [hep-ph]].
- [31] For example, A. Martin and V. Sanz, JHEP **1001**, 075 (2010) [arXiv:0907.3931 [hep-ph]].
A. Atre, G. Azuelos, M. Carena, T. Han, E. Ozcan, J. Santiago and G. Unel, JHEP **1108**, 080 (2011) [arXiv:1102.1987 [hep-ph]].
- [32] R. V. Harlander and T. Neumann, arXiv:1308.2225 [hep-ph].
- [33] R. K. Ellis, I. Hinchliffe, M. Soldate and J. J. van der Bij, Nucl. Phys. B **297**, 221 (1988).
- [34] U. Baur and E. W. N. Glover, Nucl. Phys. B **339**, 38 (1990).
- [35] G. Corcella, I. G. Knowles, G. Marchesini, S. Moretti, K. Odagiri, P. Richardson, M. H. Seymour and B. R. Webber, JHEP **0101**, 010 (2001) [hep-ph/0011363].
- [36] G. P. Salam and J. Rojo, Comput. Phys. Commun. **180**, 120 (2009) [arXiv:0804.3755 [hep-ph]].
A. Vogt, S. Moch and J. A. M. Vermaseren, Nucl. Phys. B **691**, 129 (2004) [hep-ph/0404111].
S. Moch, J. A. M. Vermaseren and A. Vogt, Nucl. Phys. B **688**, 101 (2004) [hep-ph/0403192].
T. Gehrmann and E. Remiddi, Comput. Phys. Commun. **144**, 200 (2002) [hep-ph/0111255].
M. Buza, Y. Matiounine, J. Smith, R. Migneron and W. L. van Neerven, Nucl. Phys. B **472**, 611 (1996) [hep-ph/9601302].
M. Buza, Y. Matiounine, J. Smith and W. L. van Neerven, Eur. Phys. J. C **1**, 301 (1998) [hep-ph/9612398].
W. L. van Neerven and A. Vogt, Nucl. Phys. B **568**, 263 (2000) [hep-ph/9907472].
W. L. van Neerven and A. Vogt, Nucl. Phys. B **588**, 345 (2000) [hep-ph/0006154].
W. L. van Neerven and A. Vogt, Phys. Lett. B **490**, 111 (2000) [hep-ph/0007362].
- [37] M. R. Whalley, D. Bourilkov and R. C. Group, hep-ph/0508110. Also see <http://hepforge.cedar.ac.uk/lhapdf/>
- [38] J. M. Campbell, hep-ph/0105226. R. K. Ellis, Nucl. Phys. Proc. Suppl. **160**, 170 (2006).
J. M. Campbell and R. K. Ellis, Nucl. Phys. Proc. Suppl. **205-206**, 10 (2010) [arXiv:1007.3492 [hep-ph]].
J. M. Campbell, R. K. Ellis and C. Williams, JHEP **1107**, 018 (2011) [arXiv:1105.0020 [hep-ph]].
J. M. Campbell, R. K. Ellis, R. Frederix, P. Nason, C. Oleari and C. Williams, JHEP **1207**, 092 (2012) [arXiv:1202.5475 [hep-ph]].
- [39] T. Sjostrand, S. Mrenna and P. Z. Skands, JHEP **0605** (2006) 026 [hep-ph/0603175].
- [40] E. Bagnaschi, G. Degrossi, P. Slavich and A. Vicini, JHEP **1202** (2012) 088 [arXiv:1111.2854 [hep-ph]].
- [41] From Version 4.08, see <http://www.hep.phy.cam.ac.uk/theory/webber/MCatNLO/>

- [42] A. D. Martin, W. J. Stirling, R. S. Thorne and G. Watt, *Eur. Phys. J. C* **63**, 189 (2009) [arXiv:0901.0002 [hep-ph]].
- [43] P. M. Nadolsky, H. -L. Lai, Q. -H. Cao, J. Huston, J. Pumplin, D. Stump, W. -K. Tung and C. -P. Yuan, *Phys. Rev. D* **78**, 013004 (2008) [arXiv:0802.0007 [hep-ph]].
- [44] R. V. Harlander, T. Neumann, K. J. Ozeren and M. Wiesemann, *JHEP* **1208**, 139 (2012) [arXiv:1206.0157 [hep-ph]].
- [45] A. Banfi, G. P. Salam and G. Zanderighi, *JHEP* **1206**, 159 (2012) [arXiv:1203.5773 [hep-ph]].
- [46] H. -C. Cheng, B. A. Dobrescu and C. T. Hill, *Nucl. Phys. B* **589**, 249 (2000) [hep-ph/9912343].
- [47] N. Rius and V. Sanz, *Phys. Rev. D* **64**, 075006 (2001) [hep-ph/0103086].
- [48] M. S. Carena, E. Ponton, J. Santiago and C. E. M. Wagner, *Nucl. Phys. B* **759**, 202 (2006) [hep-ph/0607106].
- [49] R. Contino, L. Da Rold and A. Pomarol, *Phys. Rev. D* **75**, 055014 (2007) [hep-ph/0612048].
- [50] G. Burdman and L. Da Rold, *JHEP* **0712**, 086 (2007) [arXiv:0710.0623 [hep-ph]].
- [51] C. T. Hill, *Phys. Lett. B* **266**, 419 (1991).